Thickness Optimization Simulation to Minimize Effective Reflectance in Broadband for SiO_2/TiO_2 Anti-Reflection Coating on Silicon Solar Cells

Jong-Chol Kim[a,*], Yun Ri[a], Un-Song Pak[b], Kyong-Chol Kim[c] and Hyok-Chang Kwon[d]

[a] *Institute of Silicate Engineering, National Academy of Science, Pyongyang, Democratic People's Republic of Korea*
[b] *Pyongyang Transportation University, Pyongyang, Democratic People's Republic of Korea*
[c] *Faculty of Applied Chemical Engineering, Kim Chaek University of Technology, Pyongyang, Democratic People's Republic of Korea*
[d] *Institute of Intelligent Information Technology, National Academy of Science, Pyongyang, Democratic People's Republic of Korea*

Received: 26.10.2021 & Accepted: 14.04.2022

Doi: 10.12693/APhysPolA.141.557 *e-mail: 15702450461@163.com

By the finite-difference time-domain method, we modeled the reflection coefficient with the ratios of the layer thicknesses of SiO_2/TiO_2. SiO_2/TiO_2 thin film thickness ratios that minimize the effective reflectance in the broadband of 400–800 nm were simulated using an artificial neural network. For the $Si/SiO_2/TiO_2$ system, the results were obtained with the following layer parameters: n(Si)= 3.7–5.6, $n(TiO_2)$ = 2.3–2.7, $d(TiO_2)$ = 25 nm, and $n(SiO_2)$ = 1.5, $d(SiO_2)$ = 24 nm. The average effective reflectance coefficient in the broadband of 400-800 nm was about 6.6%. Accordingly, the optimization of the thickness parameters of the anti-reflection film has shown that it is possible to significantly reduce the total effective reflectance in the visible range, thereby increasing the efficiency of the solar cells.

topics: silicon solar cell, FDTD, neural network, effective reflectance

1. Introduction

Anti-reflection (AR) films are widely used in many optical applications such as display panels, optical lenses, greenhouses, solar collectors, solar cells, high power lasers, and so on [1, 2]. Traditional anti-reflection coatings (ARC) are usually composed of thin film with different refractive indices. ARC performance is affected by the refractive index and thickness of each sublayer of the films [3]. ARCs films are typically applied using sol-gel spin coating, thermal evaporation, reactive sputtering, and plasma-enhanced chemical vapor deposition etc. [4].

Various materials such as SiO_2, Al_2O_3, TiO_2, SiN_x, ZnO can be used as ARCs in silicon solar cells due to the suitable refractive index of these materials [5–8]. Most crystalline silicon solar cells manufactured today contain SiN_x as a simple single-layer coating, despite toxic and hazardous gases such as SiH_4 and NH_3 used in plasma-enhanced chemical vapor deposition processes [9]. The SiN_x film is obtained by a relatively expensive method, while the TiO_2 film is obtained by cheaper environment-friendly methods. TiO_2 is one of the most widely used materials for ARCs due to its advantages such as high refractive index, excellent transmittance, chemical, stability and good mechanical properties [10]. TiO_2 can be deposited by a number of general techniques, including spin-coating of sol-gel or atmospheric pressure chemical vapour deposition (APCVD) [11, 12]. One of the advantages of TiO_2 film can decompose organic contaminants or kill bacteria adhering to surface under ultraviolet (UV) illumination [13, 14].

TiO_2-based coatings can be easily applied to transparent substrates such as glass and plastics to provide a self-cleaning function. However, the coatings developed so far always enhance surface reflection due to the large refractive index of TiO_2 ($n \approx 2.52$ for anatase, $n \approx 2.76$ for rutile) [15]. Therefore, ARCs consisting of SiO_2/TiO_2 multilayers were studied for photovoltaic (PV) applications [16]. SiO_2 thin films are typically used as a layer with a low refractive index and good light transmittance. The SiO_2 also has good passivation and scratch resistant properties and chemical stability.

When the optical thickness of each layer is $\lambda/4$, the reflection at different interfaces within ARCs interferes destructively. However, these kinds of ARCs generally work in narrow bands that cover only a small portion of the solar spectrum. The manufacture of AR films involves precise control of the refractive index and thickness of each layer of the films [17]. In 2021, Sholpan Nauryzbekova et al. [18] simulated the optimal thickness of SiO_2 and TiO_2 thin films that minimize reflection at some specific wavelength values by the finite-difference time-domain (FDTD) method (Lumerical FDTD Solutions). The Lumerical FDTD program is the world's first multiphysics suite, often used to study optical characteristics [19].

The aim of this study is to propose a simulation method to obtain the minimum thickness of a multilayer AR film, which can minimize the effective reflectance in the broadband rather than a specific or local wavelength. In the simulation, the TiO_2 layer is the outer layer of ARCs in contact with air.

The reflection coefficients with thickness ratios of the SiO_2/TiO_2 layer coated on the silicon substrate were calculated by FDTD. Then, by the artificial neural network method, the thickness ratio of SiO_2 and TiO_2 layers was obtained, where the average effective reflectance coefficient was the lowest in the range of 400–800 nm.

2. Modeling

2.1. Optimal thickness range of ARC

In the case of a single-layer ARC, the thickness and refractive index of the coating with minimal reflection at wavelength λ can be obtained from the following formula

$$\lambda/4 = 4nd,$$

where λ is the wavelength of the incident light, n and d are the refractive index and layer thickness, respectively.

In the case of a typical double-layered ARC, the thickness of each coating layer must satisfy the following equation for each layer to obtain a zero reflectance at a wavelength λ [20], i.e.,

$$d_1 = \frac{\lambda}{2\pi n_1} \tan^{-1}\left(\pm\sqrt{\frac{(n_s - n_0)(n_0 n_p - n_2^2)\, n_1^2}{(n_1^2 n_s - n_0 n_2^2)(n_1^2 - n_0 n_s)}}\right), \tag{2}$$

$$d_2 = \frac{\lambda}{2\pi n_2} \tan^{-1}\left(\pm\sqrt{\frac{(n_s - n_0)(n_0 n_s - n_1^2)\, n_2^2}{(n_1^2 n_s - n_0 n_2^2)(n_2^2 - n_0 n_s)}}\right), \tag{3}$$

where d_1 and d_2 represent the thickness of the outer and inner layers, respectively. Also, n_0, n_s, n_1 and n_2 correspond to the refractive index of the air, substrate, outer and inner layers, respectively. By the above equations, the limits of d_1 and d_2 were determined, where the reflection is minimized between the wavelengths of 400–800 nm. Refractive indices for SiO_2, TiO_2, and Si were obtained from [21–23].

2.2. FDTD simulation

To obtain the reflection coefficient with thickness ratios of the SiO_2TiO_2 film, we simulated the optical properties numerically with the Lumerical FDTD program. A schematic diagram of the simulation is shown in Fig. 1 [10].

A plane wave source in the wavelength range 400–800 nm is placed above the top surface of the TiO_2 film, and a reflection monitor (frequency domain field and power monitor) is placed above the light source. A plane wave of 400–800 nm propagates downwards to the ARC structure, where both specular and diffuse reflections are collected by the reflection monitor. The field profile monitor (frequency domain field and power monitor) is perpendicular to the surface of the substrate. The thickness of the Si substrate was 2 μm [18].

2.3. Artificial neural network model

Due to the nonlinearly changing, depending on the wavelength, the reflection coefficient of the SiO_2/TiO_2 film coated on the silicon substrate, it is difficult to obtain the thickness of the individual AR layers, whose effective reflectance is minimized in the broadband of 400–800 nm. The artificial neural network (ANN) method is used to estimate complex nonlinear problems, and the most commonly used form of ANN is BP Artificial Neural Network (BPNN). In this paper, BPNN (BP Neural Network) is used to build the optimal thickness prediction model of ARC. The BP model includes an input layer, an output layer, and one hidden layer. The thickness of the SiO_2 and TiO_2 layers was used for the input data and the effective reflectance was used for the output data. The number of neurons in the hidden layer of BPNN is as follows [24, 25]

$$P_H = \sqrt{n_I + m_O} + \alpha, \tag{4}$$

where P_H is the neuron number of the hidden layer, n_I is the neuron number of input layer, m_O is the neuron number of output layer, α is an integer between 1–10. In this modeling, the number of neurons input layer as 2, the number of neurons in the output layer as 1. According to (4), the number of neurons in the hidden layer is determined as 10.

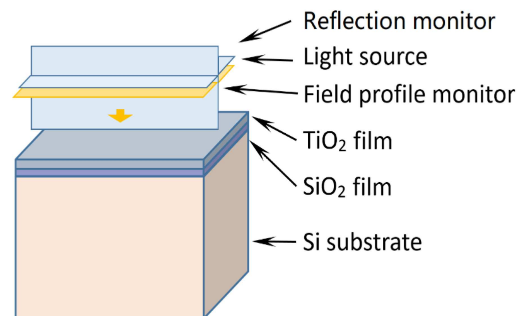

Fig. 1. Scheme of the system configuration in FDTD simulation.

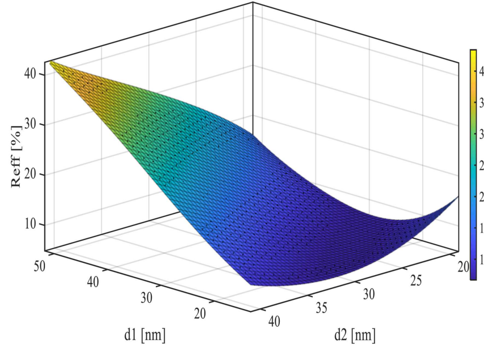

Fig. 2. The average effective reflectance coefficient in accordance with the thickness ratios of the SiO_2/TiO_2 film.

With (5) and (6), the output model of the hidden layer neuron and the output layer neuron can be calculated

$$q_j = f\left(\sum Q_i\, \mathrm{IW}_{ij} - r_j\right), \tag{5}$$

where IW_{ij} is the weight between i-th neuron of the input layer and j-th neuron of the hidden layer, r_j is j-th threshold value of hidden layer, Q_i is the i-th parameter of the input variables vector, $f(\cdot)$ is the neuron transfer function in the hidden layer.

The logsig and tansig functions are widely used as the transfer function of the hidden layer. In this paper, the logsig function is used as the transfer function

$$G_k = F\left(\sum q_j\, \mathrm{LW}_{jk} - b_k\right), \tag{6}$$

where LW_{jk} is the weight between j-th neuron of the hidden layer and k-th neuron of the output layer, b_k is k-th threshold value of the output layer, $F(\cdot)$ is the neuron transfer function of the output layer.

If the difference between the model outputs and the expected values exceeds the expected error value, a gradient search technique is applied to adjust the weight and threshold values, and then the outputs are recalculated. This process is repeated until the difference between the model output values and expected values is less than the expected error value.

3. Results

The thickness limits of the SiO_2/TiO_2 film were calculated for FDTD modeling. The limits of the thickness ratios of the SiO_2/TiO_2 film was calculated by (2) and (3). In the calculation, the wavelength (λ) is 400–800 nm, and the refractive index of air (n_0) is 1. In addition, the refractive indices (n_1, n_2, n_s) of TiO_2, SiO_2 and Si are 2.7–2.34, 1.5–1.47 and 5.7–3.7 depending on the wavelength λ, respectively [21]. The results are as follows

$$15 < d_1 < 50 \quad \text{and} \quad 20 < d_2 < 60, \tag{7}$$

where d_1 [nm] and d_2 [nm] are the thickness of the TiO_2 layer and the SiO_2 layer, respectively.

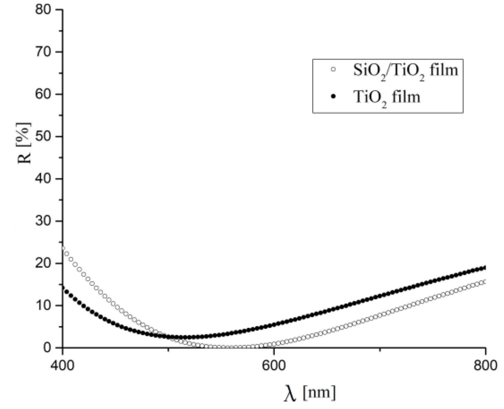

Fig. 3. The reflectance R of silicon solar cells with TiO_2 single-layer ARC and SiO_2/TiO_2 double-layer ARC, respectively, as a function of wavelength λ.

With FDTD simulation, the reflection coefficients with changes of thicknesses d_1 and d_2 of the SiO_2/TiO_2 film were obtained. Figure 2 shows the change of average effective reflectance coefficient with the thickness ratios of the SiO_2/TiO_2 film in the broadband 400–800 nm.

In Fig. 2, d_1 and d_2 are the thicknesses of the SiO_2 and TiO_2 layers, respectively, and R_{eff} represents the average effective reflectance coefficient. The energy density distribution of the spectra under AM-1.5G standard irradiation was taken from [26]. To obtain the effective reflectance coefficient, the energy density distribution was weighted to the reflection coefficient calculated by the FDTD method. As shown in Fig. 2, the average effective reflectance coefficient changed nonlinearly with the thicknesses d_1 and d_2, and the wavelength position with the minimum reflective coefficient also shifted with the thickness d_1 and d_2.

Using FDTD, 160 sample data of the reflection coefficient with a ARC thickness ratio were obtained. Among the data, 80% of samples were used as BP neural network training samples, and 20% of samples were used as BP neural network test samples. After 943 iterations, the training value reached the best value and the training average squared error was 1.065×10^{-10}. The optimal thicknesses of the SiO_2/TiO_2 film that minimize the effective reflectance in the 400–800 nm broadband, calculated with the neural network, are $d_1 = 24.987$ nm and $d_2 = 23.898$ nm.

Figure 3 shows the reflectance of silicon solar cells with TiO_2 single-layer ARC and SiO_2/TiO_2 double-layer ARC, respectively.

In Fig. 3, the thickness of TiO_2 single-layer ARC is 46 nm, which is the optimum thickness to minimize the effective reflectance. In this case, the average effective reflectance coefficient R_{eff} is 8.7% in the 400–800 nm range. Also, when the thickness $d(TiO_2) = 25$ nm and $d(SiO_2) = 24$ nm in the SiO_2/TiO_2 double-layer ARC, the average effective reflectance coefficient R_{eff} is 6.6%.

4. Conclusion

In this paper, we simulated the optimal thickness of SiO_2/TiO_2 for silicon solar cells with the FDTD and BPNN methods. In the simulations using the FDTD program, the reflection coefficients of SiO_2/TiO_2 ARCs for silicon solar cells in the range of 400–800 nm were obtained. Subsequently, using the BP neural network, the thickness of the SiO_2/TiO_2 layer with the smallest average effective reflectance coefficient in the range of 400–800 nm was simulated.

The simulation results show that thickness parameters of the SiO_2/TiO_2 layer with the lowest average effective reflectance coefficient of the $Si/SiO_2/TiO_2$ system are about 6.6% for $d(TiO_2) = 25$ nm and $d(SiO_2) = 24$ nm. Therefore, for silicon solar cells, the average effective reflectance coefficient of SiO_2/TiO_2 double-layer is 2.1% lower than of TiO_2 single-layer. These results clearly show that SiO_2/TiO_2 double-ARCs can improve the AR efficiency of silicon solar cells compared to single-layer TiO_2 ARCs. The results also show that the thickness parameters of multi-layered ARCs can be effectively optimized by FDTD and ANN simulations.

References

[1] Y.D. Xu, C. Peng, C.F. Xin, J.Q. Wu, *Mater. Lett.* **94**, 89 (2013).

[2] H. Zhang, D.-W. Fan, T.-Z. Yu, C.-L. Wang, *Chin. J. Chem. Phys.* **28**, 777 (2015).

[3] C. Xiong, W.L. Xu, Y. Zhao, J. Xiao, X.F, Zhu, *Mod. Phys. Lett. B* **31**, 1740028 (2017).

[4] A.S. Sarkın, N. Ekren, Ş. Sağlam, *Sol. Energy* **199**, 63 (2020).

[5] E.Z. Shi, L.H. Zhang, Z. Li et al., *Sci. Rep.* **2**, 884 (2012).

[6] H. Kanda, A. Uzum, N. Harano, S. Yoshinaga, Y. Ishikawa, Y. Uraoka, H. Fukui, T. Harada, S. Ito, *Energy Sci. Eng.* **4**, 269 (2016).

[7] I.S. Yu, S.C. Wu, L. Dumont, J. Cardin, C. Labbe, F. Gourbilleau, *J. Rare Earths* **37**, 515 (2019).

[8] Y.J. Lee, D.S. Ruby, D. W. Peters, B.B. McKenzie, J.W.P. Hsu, *Nano Lett.* **8**, 1501 (2008).

[9] M. J. Kerr, J. Schmidt, A. Cuevas, *J. Appl. Phys.* **89**, 3821 (2001).

[10] C.L. Wang, X.T. Zhang, S. Gao, Y. Meng, A. Fujishima, *Opt. Express* **26**, 31917 (2018).

[11] B.S. Richards, *Prog. Photovolt. Res. Appl.* **12**, 253 (2004).

[12] A. F. Thomson, K. R. McIntosh, *Prog. Photovolt. Res. Appl.* **20**, 343 (2012).

[13] T. Minabe, D.A. Tryk, P. Sawunyama, Y. Kikuchi, K. Hashimoto, A. Fujishima, *J. Photochem. Photobiol. A: Chem.* **137**, 53 (2000).

[14] Y. Kikuchi, K. Sunada, T. Iyoda, K. Hashimoto, A. Fujishima, *J. Photochem. Photobiol. A: Chem.* **106**, 51 (1997).

[15] X.T. Zhang, O. Sato, M. Taguchi, Y. Einaga, T. Murakami, A. Fujishima, *Chem. Mater.* **17**, 696 (2005).

[16] D.F. Zambrano, R. Villarroel, N. Carvajal et al., *Sol. Energy Mater. Sol. Cells* **220** (2021) 110841.

[17] X.D. Wang, J. Shen, *J. Sol-Gel Sci. Technol.* **53**, 322 (2010).

[18] S. Nauryzbekova, K. Nussupov, D. Bakranova, *Mater. Today: Proc.* **49**, 2474 (2022).

[19] D. Visser, D.Y. Chen, Y. Désières, A.P. Ravishankar, S. Anand, *Sci. Rep.* **10**, 12527 (2020).

[20] S.Y. Lien, D.S. Wuu, W.C. Yeh, J.C. Liu, *Sol. Energy Mater. Sol. Cells* **90**, 16 (2006) 2710-2719. .

[21] C. Schinke, P.C. Peest, J. Schmidt et al., *Aip Adv.* **5**, 6 (2015).

[22] S. Sarkar, V. Gupta, M. Kumar, J. Schubert, P. T. Probst, J. Joseph, T.A. König, *ACS Appl. Mater. Interface* **11**, 13752 (2019).

[23] L. Gao, F. Lemarchand, M. Lequime, *J. Europ. Opt. Rap. Public.* **8**, 13010 (2013).

[24] Y. Hu, C.D. Xiao, Y.Y. Shi, *J. Brazil. Soc. Mech. Sci. Eng.* **40**, 251 (2018).

[25] C. Kwon, U. Song, U. Pak, C.M. Kim, *J. Indian Chem. Soc.* **98**, 100042 (2021).

[26] C.A. Gueymard, D. Myers, K. Emery, *Solar Energy* **73**, 443 (2002).